

# Quench induced Mott insulator to superfluid quantum phase transition

Jay D. Sau,<sup>1</sup> Bin Wang,<sup>1</sup> and S. Das Sarma<sup>1</sup>

<sup>1</sup>*Condensed Matter Theory Center and Joint Quantum Institute, Department of Physics,  
University of Maryland, College Park, Maryland 20742-4111, USA*

Mott insulator to superfluid quenches have been used by recent experiments to generate exotic superfluid phases. While the final Hamiltonian following the sudden quench is that of a superfluid, it is not a priori clear how close the final state of the system approaches the ground state of the superfluid Hamiltonian. To understand the nature of the final state we calculate the temporal evolution of the momentum distribution following a Mott insulator to superfluid quench. Using the numerical infinite time-evolving block decimation approach and the analytical rotor model approximation we establish that the one and two dimensional Mott insulators following the quench equilibrate to thermal states with spatially short-ranged coherence peaks in the final momentum distribution and therefore are not strict superfluids. However, in three dimensions we find a divergence in the momentum distribution indicating the emergence of true superfluid order.

PACS numbers: 03.75.Kk, 05.30.Rt

*Introduction* Systems of ultra-cold atoms provide us with many-body systems with tunable Hamiltonians that may potentially be used to realize various quantum phases of matter. However many of the interesting phases that have been predicted require extremely low temperatures that have not been reached in experiments. One new phase of matter that has been realized in cold atomic systems is the Mott-insulator (MI) phase, which is a gapped collective phase and therefore has the special property of a low entropy-density. This low entropy density makes the MI a favorable starting point for creating other low-temperature phases of atoms. In particular, a recent set of experiments [1] uses an effective Mott phase as a starting state and suddenly ramps up the tunneling to create potentially exotic low temperature superfluid-like (SF) states with  $p$  and  $f$ -orbital symmetries that have never been realized before. While such a sudden change or quench of the Hamiltonian from an initially known state to a desired Hamiltonian is a promising way to realize new states of matter [2, 3], it is not clear whether a system following the quench evolves to a state near the desired ground state phase in any sense. Since the quenching process is manifestly non-adiabatic and very far from equilibrium, it is certainly possible, perhaps even likely, that the final state has only a small overlap with the ground state of the final Hamiltonian! Measurements of the momentum density using time-of-flight imaging do indeed show that the initially uniform momentum distribution, which characterizes the MI phase, develops coherence peaks that are characteristic of the superfluid phase. However, this evolution where the momentum density bunches up into peaks instead of spreading out is counter-intuitive and suggests dissipation of energy similar to evaporative cooling that is used to create Bose-Einstein condensates (BECs). Therefore, to understand the utility of this approach to realizing new phases of ultra-cold atoms, it is necessary to understand both the origin and extent of the superfluid state that is formed following similar quenches.

A natural approach to understanding these quenches is to consider an analogous quench in the most studied and simplest transition that has been observed in ultra-cold atomic

systems, namely the MI to SF phase transition in  $s$ -wave optical lattices [4]. While there have been several theoretical studies of quenches in optical lattices from the SF to the MI phase [5], studies on quenches from the MI to the SF phases have been restricted to either infinite dimensions or one dimension. These calculations have mostly focused on the development of local phase coherence and entanglement in real space which is a particularly interesting aspect of MI to SF quenches [6, 7]. However, the local phase coherence and the entanglement do not completely characterize the final state of the system reached. In particular they contain only indirect information about the long-range coherence that is measured by time-of-flight imaging. Therefore some very recent works [8, 9] have concentrated on comparing the time-of-flight measurements in quench experiments with theoretical estimates of the momentum density.

In this letter we develop an understanding of the peak formation in momentum distribution following an MI-SF quench by calculating this distribution for bosonic atoms trapped in an  $s$ -wave optical lattice. Since the initial MI phase is completely incoherent between sites, the momentum distribution is uniform. To reach a SF state, the tunneling is instantaneously quenched to a finite value on the SF side of the ground-state phase diagram. We find that the momentum distribution after the quench depends strongly on the dimensionality of the lattice under consideration. The simplest case is the zero-dimensional lattice, where the momentum density following the MI-SF quench continues to oscillate in time and thus does not appear to equilibrate. In contrast, the one-dimensional MI chain, whose dynamics we calculate numerically using the systematically exact infinite time-evolving block decimation (iTEBD) [10] approach yields a momentum distribution which approaches equilibrium. Furthermore, the dynamics of the momentum density qualitatively agrees with the distribution calculated from the quantum rotor model (exact in the large filling limit) [11, 12] studied within the semi-classical truncated Wigner approximation (TWA)[13]. Moreover, the equilibrium momentum density estimated from iTEBD quantitatively agrees with the result from the classical rotor model.

Using this fact, which we verified in zero and one dimensions, we estimate the equilibrium momentum density using the classical rotor approximation in two and three dimensions following a quench. Both these cases are relevant to the recent experiments [1]. We find that such an MI-SF quench in the two dimensional limit leads to a classical thermal gas state with short-ranged momentum correlations (and no condensate fraction). On the other hand, an MI-SF quench in the three dimensional case, which directly applies to the experimental results, yields a true condensate.

*Quenches in the Bose Hubbard model:* Ultra-cold bosonic atoms in a deep optical lattice can be described by the Bose-Hubbard model which is written as

$$H = -\zeta \sum_{\langle i,j \rangle} (b_i^\dagger b_j + h.c.) + \frac{U}{2} \sum_j n_j(n_j - 1), \quad (1)$$

where  $\langle i, j \rangle$  are nearest neighbor sites on the optical lattice,  $b_j^\dagger$  is the boson creation operator on site  $j$ ,  $n_j = b_j^\dagger b_j$  is the number operator of bosons on site  $j$  and  $U$  is the charging energy per site. The inter-site tunneling matrix element  $\zeta$  between the sites is taken to vanish in the initial state so that the system is initially in a MI ground state with  $\langle n_j \rangle = n$  (integer) atoms per site. The momentum distribution of the bosons, that is measured by time-of-flight images, is the fourier transform of the off-diagonal density matrix

$$n_k = \sum_j e^{ikj} \langle b_j^\dagger b_0 \rangle. \quad (2)$$

If we assume that the state following the quench reaches a thermal equilibrium, then the correlations can be calculated from the free energy

$$F[\beta, \mu] = -\frac{1}{\beta} \log \text{Tr}(e^{-\beta H - \mu N}) \quad (3)$$

where the inverse final temperature  $\beta$  and chemical potential  $\mu$  are determined by the conserved initial energy  $\langle E \rangle = -\partial_\beta(\beta F) = 0$  and  $\langle N \rangle = -\beta \partial_\mu F = n$ .

*Zero-dimensional quenches:* Let us start by considering the simplest MI-SF quench of a zero-dimensional MI which has two sites connected by a bond. This corresponds to the two-well Josephson case [12]. The Hamiltonian  $H$  for such a system can be numerically diagonalized exactly for various filling factors to obtain both the equilibrium value and dynamics of the momentum distributions  $n_k$ , which we plot in Fig. 1. For convenience we focus on the ‘‘visibility’’ of the momentum distribution,

$$\text{Visibility} = \frac{2(n(k=0) - n(k=\pi/a))}{(n(k=0) + n(k=\pi/a))}, \quad (4)$$

which is a measure of how peaked the momentum distribution is at its maximum at  $k=0$  compared to its minimum at  $k=\pi/a$  ( $a$  being the lattice constant of the optical lattice).

An interesting feature of the zero-dimensional MI-SF quench which is seen in Fig. 1(b) is that the visibility does not

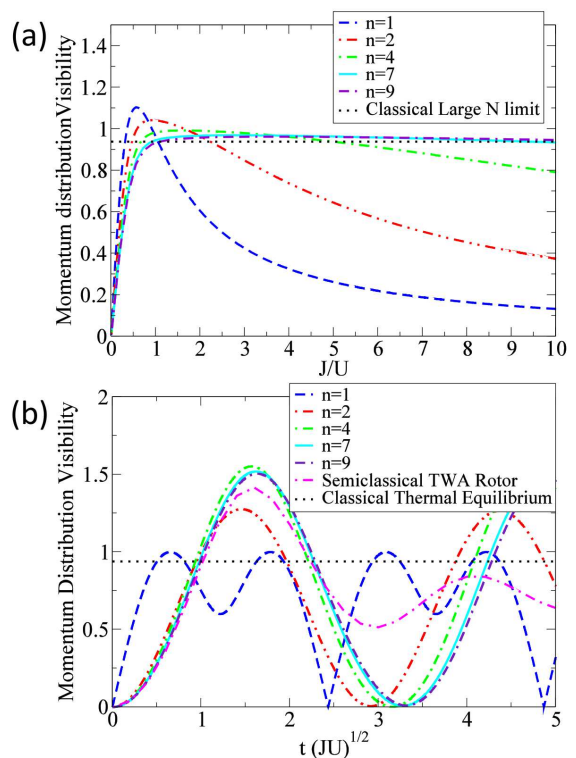


FIG. 1: (a) Equilibrium visibility of momentum distribution (defined in Eq. 4) following a quench in a 0D (2 site) Mott insulator from  $J_{initial} = 0$  to  $J_{final} = J$  at various fillings  $n$  as a function of  $J/U$ . Equilibrium is assumed to be thermal. Results at large filling  $n$  agree well with the rotor value. (b) Quantum dynamics simulations of visibility for 0D system show absence of equilibration.

equilibrate to an equilibrium value. Fortunately, we find that this lack of equilibration following the MI-SF quench is restricted to the zero-dimension case, while higher dimensional MIs reach the thermal equilibrium states in Eq. 3. Therefore it is useful to consider the results of the thermal distribution in Fig. 1(a). The equilibrium visibility for various fillings  $n$  starts close to zero for small final values of the Josephson coupling  $J = 2n\zeta$  corresponding to weak tunneling  $\zeta$  in the MI phase and rapidly rises to a certain nearly universal value before falling off at larger tunneling.

The range of intermediate  $J/U$  for which the universal visibility is attained increases with  $n$ , suggesting that the intermediate  $J/U$  values are described by a large  $n$  limit corresponding to the quantum rotor model:

$$H_{rot} = -J \sum_{\langle ij \rangle} \cos(\phi_i - \phi_j) + \frac{U}{2} \sum_j \pi_j^2 \quad (5)$$

where  $\pi_j = -i\partial_{\phi_j}$  is the angular momentum canonically conjugate to  $\phi_j$  [11, 12]. The free-energy  $F$  is approximated by replacing  $H \rightarrow H_{rot}$  in Eq. 3. At values of  $J$  comparable to the Mott-gap  $U$ , the system equilibrates to a sufficiently high temperature  $\beta^{-1}$ , so that the free-energy  $F$  in the classical limit is a combination ( $F = -\frac{\log Z_{XY}}{\beta} + \frac{\log \beta}{2\beta}$ ) of charge fluctu-

tuations with energy  $\frac{1}{2\beta}$  and phase fluctuations described the classical XY model

$$H_{XY} = -J \sum_{\langle ij \rangle} \cos(\phi_i - \phi_j) \quad (6)$$

where  $Z_{XY} = \int \prod_j \phi_j e^{-\beta H_{XY}}$  is the partition function of the XY model. In this approximation, the final temperature  $\beta^{-1}$  is determined by the equation

$$Z_{XY}^{-1} \int \prod_j d\phi_j \cos(\phi_1 - \phi_0) e^{\tilde{J} \sum_{\langle j,k \rangle} \cos(\phi_j - \phi_k)} = \frac{1}{2d\tilde{J}} \quad (7)$$

where  $\tilde{J} = \beta J$  and  $d$  is the average coordination number of each site of the lattice under consideration. For the zero-dimensional lattice  $d = 1$  (after dropping a global  $U(1)$  degree of freedom). The equilibrium momentum distribution  $n_k$  is given by the Fourier transform of the real-space correlation function (see Eq. 2)

$$\langle b_j^\dagger b_0 \rangle \propto \langle e^{i(\phi_j - \phi_0)} \rangle = \int \frac{\prod_l d\phi_l}{Z_{XY}} e^{i(\phi_j - \phi_0)} e^{\tilde{J} \sum_{\langle l,l' \rangle} \cos(\phi_l - \phi_{l'})}. \quad (8)$$

Within the XY-model approximation, the coherent momentum distribution peak results from a dissipation of phase fluctuation energy  $H_{XY}$  in the initial state into charge fluctuation energy in the final state. The zero-dimensional MI equilibrium is given by  $\tilde{J} = 1.065$  so that one has an equilibrium visibility of = 0.939. As is clear from Fig. 1(a), the equilibrium visibility is in good agreement with the large  $n$  equilibrium. At large values of  $J$ , fluctuations in the number density ( $|(n_j - n) = \pi_j| \gtrsim n$ ) lead to a break-down of the simple rotor approximation  $H_{rot}$ .

**1D Mott insulators:** Unlike the zero-dimensional MI, the one-dimensional MI cannot be solved by exact diagonalization. Therefore, we calculate the momentum distribution  $n_k$  using the in principle exact iTEBD method. As seen in Fig. 2(b), the calculated visibility in this case, in contrast to the zero-dimensional MI, approaches equilibrium values. This is qualitatively similar to the semiclassical dynamics associated with the quantum rotor model  $H_{rot}$  calculated within the TWA. Within the TWA, the distribution of the phases  $\phi_j$  begins with the uniform distribution for the MI phase and evolves according to the classical equations of motion [13]

$$\ddot{\phi}_j = JU \sum_i \sin(\phi_j - \phi_i). \quad (9)$$

Thus, as seen in Fig. 2(b), the time-scale for dynamics following the MI-SF quench within iTEBD and also the classical rotor approximation scales as  $\tau \propto (JU)^{-1/2}$ . However, as in the zero-dimensional case, the classical estimate for the final equilibration visibility appears to be valid only for intermediate values of  $J/U$ .

The partition function for the classical one-dimensional XY model (Eq. 6), can be written in a transfer-matrix form (see for example [14]) as

$$Z_{XY} = Tr[M^N(\phi - \phi')] \quad (10)$$

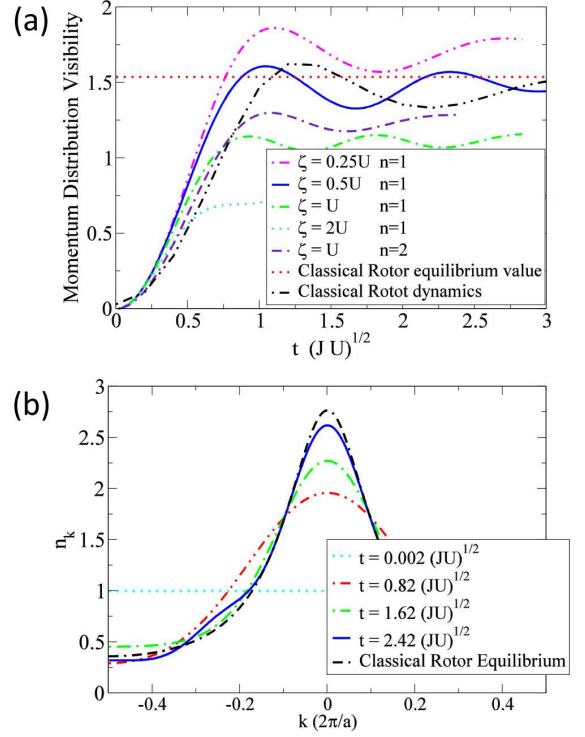


FIG. 2: (a) Quantum dynamics (iTEBD) simulations of visibility for 1D system and classical Rotor approximation show equilibration following a quench in a Mott insulator from  $J_{initial} = 0$  to  $J_{final} = J$  at various fillings  $n$  and  $J/U$ . The thermal equilibrium visibility determined from the classical rotor model is in good agreement with the iTEBD and classical dynamics results. (b) Time-evolution of the momentum distribution to one that is in good agreement with the classical thermal distribution.

where  $M(\phi) = e^{\tilde{J} \cos \phi} = \sum_n I_n(\tilde{J}) e^{in\phi}$ , and  $I_n(x)$  are modified Bessel functions. Similar to the zero-dimensional case, the one-dimensional classical equilibrium temperature is solved by  $\tilde{J} = 1.065$ . The equilibrium momentum distribution of the bosons for the  $N = \infty$  lattice is calculated to be

$$n_k = \sum_r e^{ikr} \langle e^{i(\phi_r - \phi_0)} \rangle = \frac{4\tilde{J}^2 - 1}{4\tilde{J}^2 + 1 - 4\tilde{J} \cos k}. \quad (11)$$

The classical equilibrium visibility from Eq. 4, consistent with Fig. 2(a), is found to be 1.52. Moreover, the final momentum distribution at  $n = 1, \zeta = 0.5U$  shown in Fig. 2(b) is in quantitative agreement with the classical equilibrium  $n_k$ .

**2D Mott insulators:** The classical rotor model approximation can also be used to calculate the equilibrium momentum distribution for a MI-SF quench in a two-dimensional MI at filling factors  $\bar{n} \gg 1$  in the initial state. Such a two-dimensional MI quench could be realized in experiments by adding a planar confining potential to the set-up in recent experiments [1]. Unlike the one-dimensional case, the two-dimensional XY model does not have a simple analytic so-

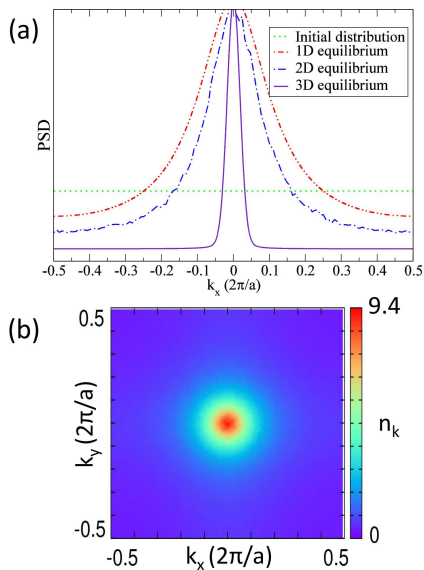


FIG. 3: (a) Equilibrium momentum density as a function of momentum  $k_x$  after an MI-SF quench as compared with the initial distribution for one-dimensional MI, two-dimensional MI and three dimensional MI. All calculated within the classical rotor model approximation. The three dimensional MI case shows the emergence of a true condensate with a divergent  $k = 0$  peak which we have broadened by  $\sigma = 0.05\pi/a$ . For convenience the momentum densities at  $k_x = 0$  has been scaled to the same value. (b) Two-dimensional momentum distribution ( $n_k$ ) following an MI-SF quench for the two-dimensional MI shows a peak at  $k_x = k_y = 0$  which is 3 times higher than the 1D peak and qualitatively resembles the peak seen in experiments [1].

lution and so we use the cluster-update Monte-Carlo (MC) scheme [15] to calculate the average energy for the two-dimensional XY model (Eq. 6) on a  $127 \times 127$  lattice with periodic boundary conditions to determine the equilibrium final temperature satisfying Eq. 7. We find the equilibrium temperature  $\beta^{-1} = 1.51J$  to be larger than the Kosterlitz-Thouless temperature  $\beta_{KT}^{-1} = 0.89J$  [16]. As seen in Fig. 3, the momentum density at  $\tilde{J} = \beta J = 0.662$  calculated using MC and Eq. 2 shows a peak at  $k = 0$  qualitatively similar to an  $s$ -wave analog of the momentum distributions observed in experiment for  $p$ -wave superfluids [1]. A section of the momentum distribution with ( $k_x = k, k_y = 0$ ) plotted as a function of  $k_x = k$  as shown in Fig. 3(a), shows a peak that is 3 times higher at  $k = 0$  than that obtained for the one-dimensional MI. However, the equilibrium momentum distributions of the quenched MI both in one and two dimensions remain finite and smooth around  $k \sim 0$  indicating a boson correlator that is exponentially decaying in real space.

**3D Mott Insulator:** The classical rotor approximation can also be applied to the three dimensional case as well. In contrast to the lower dimensional MI-SF quenches, we find that in three dimensions, the energy density  $\epsilon_{n_s} = -0.988$  at MI-SF transition calculated using MC [20] is slightly higher than the equilibrium value following the quench given by Eq. 7, indi-

ating an equilibrium phase with a true SF component. This is consistent with the high-temperature expansion for a 3D MI on a simple-cubic lattice [17] which estimates the equilibrium temperature  $\beta^{-1} \sim 2.10J$  to be below the critical temperature  $T_c = 2.202J$  [20]. Since the equilibrium temperature is close to the critical temperature, we can use scaling relations around the critical point to estimate the momentum distribution and the equilibrium temperature below  $T_c$  (where the high-T expansion is not reliable). Using the scaling relations for the energy density around  $\beta^{-1} \sim T_c$ , we obtain the equilibrium temperature  $\beta^{-1} = T_c - 0.077J$ . The momentum distribution in the vicinity of  $\beta^{-1} \lesssim T_c$  has a universal form at small  $k$  [19, 21] which is given by

$$F(k) \approx w(\beta)^2 [(2\pi)^3 \delta(\mathbf{k}) + \frac{\xi_T}{k^2}] + f_0. \quad (12)$$

Since the critical fluctuation contribution to  $n_k$  is only accurate near  $k \sim 0$ , we have added a  $k$ -independent background  $f_0 = [1 - w(T)^2(1 + \xi_T/2\pi)]$  to restore the total spectral weight to unity. Here  $w(\beta) = B \left( \frac{T_c - \beta^{-1}}{T_c} \right)^{\beta_0}$  is the condensate fraction of the system. The parameters in Eq. 12 are critical exponents and amplitudes [18] which have been calculated using both high-T scaling expansions [17] together with MC calculations to be: the critical amplitude  $B = 1.245$ , the critical exponent  $\beta_0 \approx 0.35$ , the transverse correlation length  $\xi_T(T) = \xi^{(-)} \left( \frac{T_c - T}{T_c} \right)^{-\nu}$  with  $\xi_T^{(-)} \approx 1.65$  and  $\nu \approx 0.67$  [20, 21]. To resolve the singularity at  $k \sim 0$  we have added a broadened the momentum distribution by a width  $\sigma = 0.05\pi/a$ . The resulting singular momentum distribution is plotted in Fig. 3 as a function of  $k_x = k$ , with  $k_y = k_z = 0$  has a peak near  $k \sim 0$  with total weight of  $1 - f_0 \sim 0.3$ .

The recent MI-SF quench experiments [1], in the three-dimensional limit, can be thought of as a 3D MI-SF quench where the initial state is the ground state of the 3D XY Hamiltonian (Eq. 6) with tunneling  $\zeta$  turned on only along  $z$ . This corresponds to a lower initial energy density which in turn leads to a reduced equilibrium temperature  $T_c - \beta^{-1} = 0.16J$  because of energy dissipated in the phase-fluctuations along the tube. This results peak near  $k \sim 0$  in the momentum distribution with total weight  $1 - f_0 \approx 0.6$  which is twice as large as the peak obtained from quenching from the 3D MI state.

**Conclusion:** We have calculated the formation of peaks in the momentum distribution of bosonic atoms in an optical lattice following a quench from deep in the MI phase to an SF phase within the classical (spin- $\infty$ ) XY model approximation. The classical results are in semi-quantitative agreement with exact iTEBD calculations for the one-dimensional MI. Understanding such MI-SF quenches is particularly important in the context of recent experiments that use such quenches to reach superfluid-like states. From our calculations we find that in one, two and three-dimensional MI, the initially uniform momentum distribution develops a peak at momentum  $k = 0$  following the quench that is qualitatively similar to the one in experimental time-of-flight images. However in one and two dimensions the resulting momentum distribu-

tions are non-singular at  $k = 0$  and represent phases without long-range phase order. In contrast, we find a true condensate in the three dimensional MI corresponding to the recent experiments[1] with a divergent momentum distribution at  $k = 0$ . One interesting way to verify our theoretical predictions is to use the recently developed quantum gas microscope technique [22] to look directly at the time evolution of the MI to SF quenches in systems of different dimensionalities.

We thank R. Sensarma and A. Hemmerich for introducing us to this problem. This work was supported by DARPA-OLE, JQI-NSF-PFC, ARO-MURI and AFOSR-MURI.

- 
- [1] G. Wirth, M. Ohlschlager, and A. Hemmerich, *Nat. Phys.* **7**, 147 (2011); M. Ohlschlager, G. Wirth, and A. Hemmerich, *Phys. Rev. Lett.* **106** 015302 (2011).
- [2] L. E. Sadler, J. M. Higbie, S. R. Leslie, M. Vengalattore, and D.M. Stamper-Kurn, *Nature* **443**, 312 (2006).
- [3] M. Lewenstein and W. Vincent Liu, *Nat. Phys.*, **7**, 101, (2011).
- [4] M. Greiner et al, *Nature* **415**, 39 (2002).
- [5] C. Kollath, A. Lauchli and E. Altman, *Phys. Rev. Lett.* **98**, 180601 (2007); G. Roux, *Phys. Rev. A*, **79**, 021608 (2009).
- [6] M. Rigol, A. Muramatsu, *Phys. Rev. Lett.* **94**, 240403 (2005).
- [7] P. Navez, R. Schutzhold, *Phys. Rev. A* **82**, 063603 (2010).
- [8] S. Trotzky, Y.-A. Chen, A. Flesch, I. P. McCulloch, U. Schollwöck, J. Eisert and I. Bloch, arXiv:1101.2659 (2011).
- [9] D. Chen, M. White, C. Borries, and B. DeMarco, arXiv:1103.4662 (2011).
- [10] G. Vidal, *Phys. Rev. Lett.* **98**, 070201 (2007).
- [11] U.R. Fischer, R. Schutzhold, M. Uhlmann, *Phys. Rev. A* **77**, 043615 (2008).
- [12] J. R. Anglin, P. Drummond, and A. Smerzi, *Phys. Rev. A* **64**, 063605 (2001); R. Barnett, J. D. Sau, and S. Das Sarma, *Phys. Rev. A* **82**, 031602(R) (2010).
- [13] J. D. Sau, S. R. Leslie, D. M. Stamper-Kurn, and M. L. Cohen, *Phys. Rev. A* **80**, 023622 (2009); A. Polkovnikov, *Annals of Phys.* **325**, 1790 (2010)
- [14] D.J. Scalapino, M. Sears, R. A. Ferrell, *Phys. Rev. B*, **6**,3409 (1972).
- [15] U. Wolff, *Phys. Rev. Lett.* **62**, 361 (1989).
- [16] J.M. Kosterlitz and D. J. Thouless, *J. Phys. C* **6**, 1181 (1973); J. Tobochnik and G. V. Chester, *Phys. Rev. B* **20**, 3761 (1979).
- [17] M. Ferer, M. A. Moore, M. Wortis, *Phys. Rev. B*, **8**, 5205 (1973).
- [18] A. Aharony and P. C. Hohenberg, *Phys. Rev. B* **13**, 3081 (1976).
- [19] P. C. Hohenberg, A. Aharony, B. I. Halperin and E. D. Siggia, *Phys. Rev. B* **13**, 3081 (1976).
- [20] A. Cucchieri, J. Engels, S. Holtmann, T. Mendes, T. Schulze, *J. Phys. A*, **35**,6517 (2002).
- [21] A. Pelissetto and E. Vicari, *Phys.Rept.* **368**,549 (2002).
- [22] W. S. Bakr, J. I. Gillen, A. Peng, S. Flling, and M. Greiner, *Nature* **462**, 74 (2009)